Using "Rapid Revisit" CYGNSS Wind Speed Measurements to Detect Convective Activity

Jeonghwan Park, Joel T. Johnson, *Fellow, IEEE*, Yuchan Yi, and Andrew J. O'Brien

***Abstract*—The Cyclone Global Navigation Satellite System (CYGNSS) is a spaceborne GNSS-reflectometry mission, which was launched on December 15, 2016 for ocean surface wind speed measurement. CYGNSS includes eight small satellites in the same low earth orbit, so that the mission provides wind speed products having unprecedented coverage both in time and space to study multitemporal behaviors of oceanic winds. The nature of CYGNSS coverage results in some locations on earth experiencing multiple wind speed measurements within a short period of time (a "clump" of observations in time) resulting in a "rapid revisit" series of measurements. Such observations seemingly can provide indications of regions experiencing rapid changes in wind speeds, and therefore serve as an indicator of convective activity. An initial investigation of this concept using simulated and on-orbit CYGNSS measurements is provided in this paper. The temporally "clumped" properties of CYGNSS measurements are examined, and the results show that clump durations and spacing vary with latitude. For example, the duration of a clump can extend as long as a few hours at higher latitudes, with gaps between clumps ranging from 6 to as high as 12 h depending on latitude. Initial examples are provided to indicate the potential of changes within a clump to detect convective activity through a comparison with convective activity indicators derived from model datasets. The results at present are limited by the ongoing calibration of CYGNSS wind speed retrievals, so that future work will be required to obtain a more complete assessment, but nevertheless clearly indicate the potential utility of the method for studies of atmospheric convection.**

***Index Terms*—Atmospheric convection, Cyclone Global Navigation Satellite System (CYGNSS), ocean surface wind speed measurement.**

I. Introduction

NASA'S Cyclone Global Navigation Satellite System (CYGNSS) mission [1], [2] was launched on December 15, 2016 and is currently providing GNSS-reflectometry measurements from an eight small satellite constellation in low earth orbit. CYGNSS measurements of sea surface specular reflected power are used to retrieve ocean surface wind speeds with unprecedented spatial coverage and a median revisit time of 4 h on average. Fig. 1 illustrates accumulated CYGNSS measurement locations over earth's surface for 1.5- and 24-h periods, and illustrates the extensive spatial coverage achieved. A closer examination of the temporal properties of CYGNSS sampling shows however that revisits actually occur in temporal "clumps" of closely spaced successive observations followed by longer periods with no measurements. The "rapid revisit" series of wind speed measurements obtained in a temporal clump potentially allow studies of the temporal behaviors of oceanic winds over time scales 1 h or shorter. Such observations seemingly should provide indications of regions experiencing rapid changes in wind speeds, indicating convective activity or other rapid temporal changes. In what follows, the term "convective activity" is used to refer to any atmospheric phenomena giving rise to observable changes in surface wind speeds over time scales of 1 h or less. These may include but are not limited to, wind gusts, frontal boundaries, or cyclonic events [3]–[6].

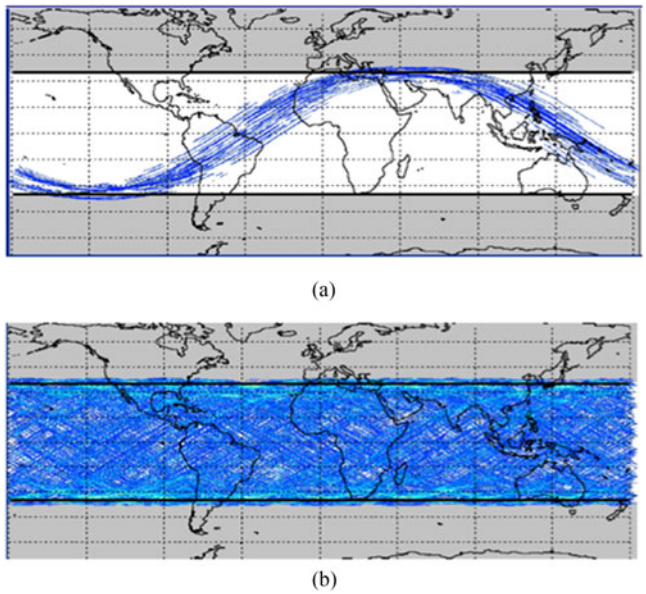

Fig. 1. Accumulated CYGNSS measurement locations over earth's surface for (a) 1.5 h and (b) 24 h (source: CYGNSS website, 2013).

This paper presents an initial examination of the use of CYGNSS rapid revisit measurements, including the characteristics of CYGNSS observation "clumps" and the initial use of CYGNSS on-orbit rapid revisit measurements to detect convective activity. The demonstrations reported here are limited by the ongoing calibration of CYGNSS wind speed retrievals, so that only a limited set of examples are shown.

Manuscript received February 20, 2018; revised May 2, 2018; accepted May 30, 2018. The research of this article is funded by NASA ROSES 2016 Weather Program Grant NNH16ZDA001N-WEATHER. *(Corresponding author: Jeonghwan Park.)*

J. Park, J. T. Johnson, and A. J. O'Brien are with the ElectroScience Laboratory, Department of Electrical and Computer Engineering, The Ohio State University, Columbus, OH 43221 USA (e-mail: park.1558@osu.edu; johnson.1374@osu.edu; obrien.200@osu.edu).

Y. Yi is with the Division of Geodetic Science, School of Earth Sciences, The Ohio State University, Columbus, OH 43210 USA (e-mail: yi.3@osu.edu).

Color versions of one or more of the figures in this paper are available online at http://ieeexplore.ieee.org.

Digital Object Identifier 10.1109/JSTARS.2018.2848267

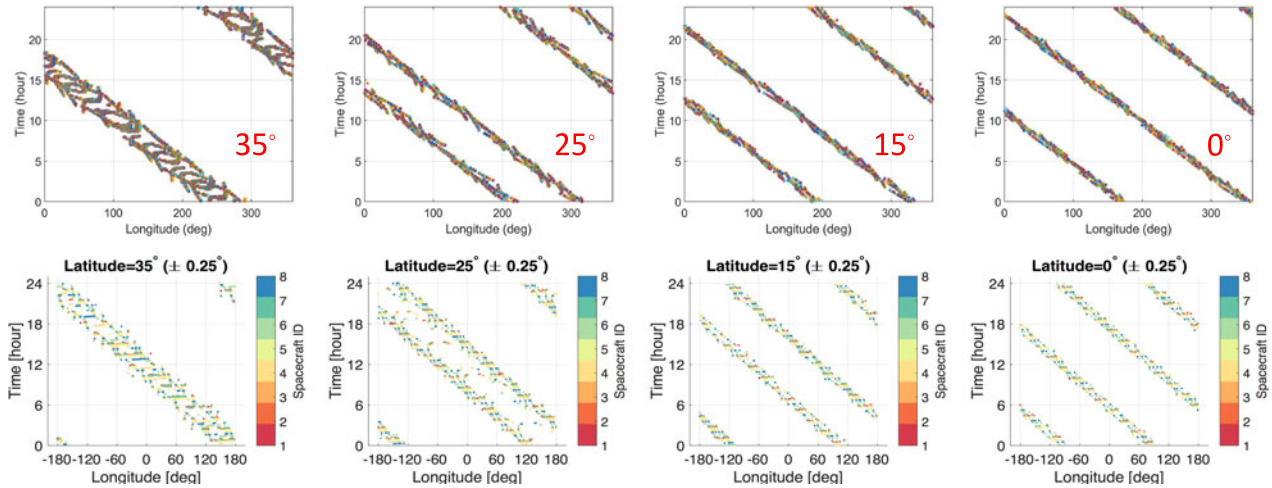

Fig. 2. One day CYGNSS observation times versus longitude for a single 0.5° × 0.5° grid cell at the indicated latitude from prelaunch simulation (top) and on-orbit measurements (bottom).

This paper is organized as follows. Section II studies the sampling properties of CYGNSS measurements in space and time using both prelaunch simulations and on-orbit measurements. Section III then reports results from a prelaunch simulation study on the use of clumped measurements to detect convective activity, and Section IV provides further information on the detection process developed for on-orbit CYGNSS data. An initial verification of convective activity detection is then described in Section V through comparisons with convective activity maps generated using atmospheric model data. Finally, Section VI provides a summary and conclusions.

II. Temporal Properties of CYGNSS Sampling

The temporal sampling characteristics provided by the CYGNSS constellation have unique properties when compared to other existing satellite wind speed measurements. CYGNSS measurements from an individual satellite occur as specular "tracks" that occur between the CYGNSS receiver and a GPS transmitter. These tracks vary due to the asynchronous orbit periods of the GPS and CYGNSS constellations, so that no consistent or repeat pattern of specular tracks occurs for a specified location on earth. However, as the eight satellite constellation sequentially overpasses a location on earth over a period of 1–2 h, multiple wind speed measurements routinely occur in a temporal clump of measurements.

In order to clarify the nature of CYGNSS sampling prior to the CYGNSS launch, a simulation of the constellation was conducted using modeled GPS and CYGNSS orbit information for the month of June 2015. The upper plots of Fig. 2 illustrate CYGNSS measurement times obtained over one day as a function of longitude at the indicated latitudes of 0°, 15°, 25°, and 35°, and show multiple measurements closely spaced in time that are then separated by a temporal gap whose duration depends on latitude. The duration of a "clump" can extend as long as a few hours at higher latitudes, with gaps between clumps that can range from as little as 6 to as high as 12 h, also depending on latitude.

In many applications, CYGNSS observations obtained within one of the clumps in time shown in Fig. 2 would be averaged and treated as a single observation. This can be advantageous if the goal is to reduce measurement error for a wind scene that is assumed to be stationary in time. However, measurements occurring in clumps whose durations can approach multiple hours seemingly offer the potential to observe wind variations on shorter time scales that may be geophysically significant. Clearly changes in winds over such time scales should be expected to be associated with rapid convection events. A rapid revisit product obtained by examining the changes in CYGNSS wind speed observations within a clump therefore may serve as a partial indicator of convective activity.

To clarify CYGNSS sampling properties further, Fig. 3 plots locations having simulated maximum clump durations of greater than 1 h, 45 min, 30 min, and 15 min. Clearly greater coverage is achieved for shorter clump periods, but the utility of such short durations becomes questionable. Fig. 3 makes clear that a rapid revisit product is most likely to contain geophysical information at latitudes near ±35°.

The lower plots of Fig. 2 were created following the process used to create the upper plots, but using CYGNSS on-orbit measurements from September 30, 2017. The similar patterns obtained confirm the insights obtained from the prelaunch simulation, although some differences are observed due to the ongoing orbit position adjustment of the CYGNSS constellation as well as the removal of CYGNSS measurements flagged as having reduced-quality retrievals.

As a further example of CYGNSS sampling, Fig. 4 provides a zoomed map for a specific location in the Indian Ocean. Using a 0.5° × 0.5° grid cell in latitude and longitude (the white dashed lines in the plot) for a 30-min period as the constellation overpasses, a maximum of 30 CYGNSS measurements from three CYGNSS satellites are obtained in one of the grid cells, with multiple other grid cells showing more than ten measurements. Figs. 5 and 6 further present the number of on-orbit samples observed during 30 min in a 0.5° grid cell in terms of a map and a histogram, respectively, using 39 200 samples obtained

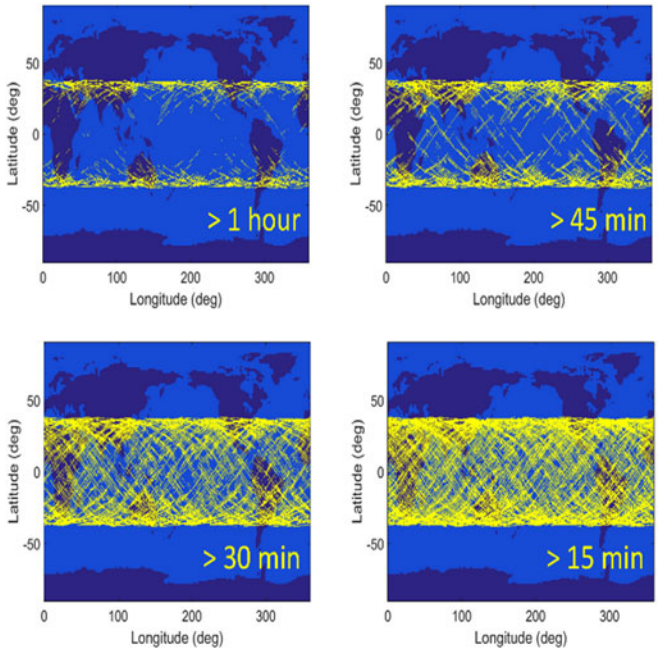

Fig. 3. Locations on 0.5° × 0.5° grid having "clumps" of greater than 1 h, 45 min, 30 min, or 15 min, for 1 day of CYGNSS measurements.

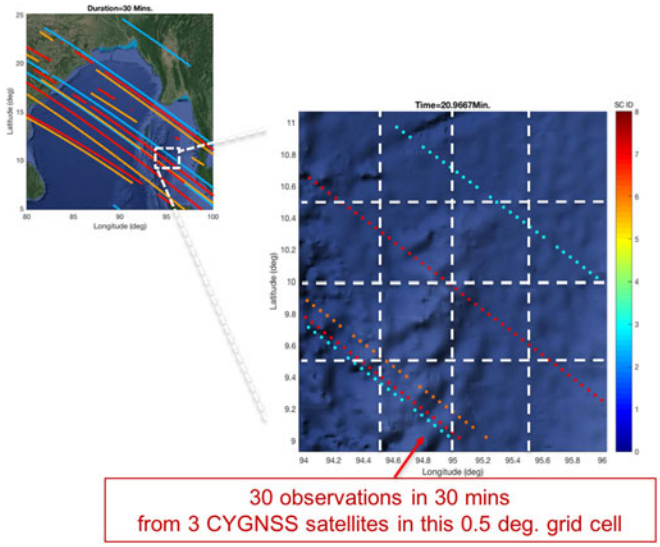

Fig. 4. Zoomed map at a specific location including 0.5° grid cells during 30 min.

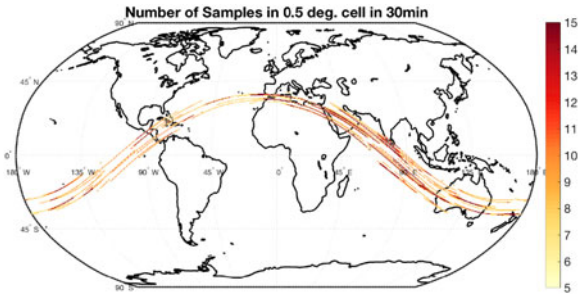

Fig. 5. Number of CYGNSS measurements in 0.5° grid cell over 30 min.

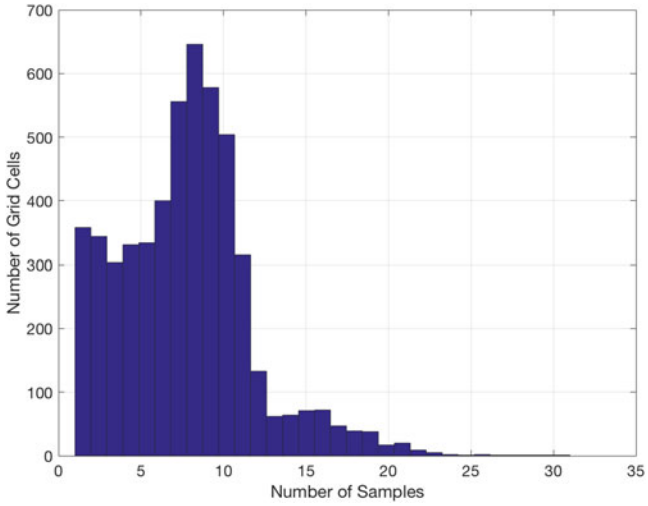

Fig. 6. Histogram of number of CYGNSS measurements in 0.5° grid cell over 30 min (total 5257 grids).

from six CYGNSS receivers and excluding flagged data. For the 5257 grid cells for which a nonzero number of measurements occurred, 7.46 samples were obtained on average with a maximum of 31 samples and a minimum of 1 sample. These results clearly show that temporal clumps of CYGNSS measurements occur frequently, motivating further examination of their use for detecting atmospheric properties. It is noted that the 0.5° resolution used in this and subsequent examples is relatively coarse as compared to the spatial scales of some convective behaviors, so that finer grid spacings are of interest, but would suffer from a smaller number of samples being obtained in a single clump. For the purposes of this initial analysis and to allow a larger number of samples, a 0.5° spatial resolution is emphasized.

III. Temporal Behaviors of Modeled Wind Fields

To develop methods for detecting convective activity from wind speed time series data, atmospheric wind fields from the CYGNSS project 13-day "Nature Run" [7] were used. This dataset provides simulated weather data (and the resulting simulated CYGNSS wind speed retrievals) for an Atlantic cyclone over 13 days (July 29–August 10). The simulated period includes the cyclone's formation and evolution, including the tropical storm (August 2), just after rapid intensification (August 4), steady state (August 6), and weakening (August 10) phases. The input geophysical data contain products at a variety of spatial and temporal resolutions; the analysis reported here was performed using the modeled wind fields at 25 km and 30-min resolutions, respectively, with an additional interpolation in time to 5-min samples. To focus on the potential value of rapid revisit analyses, the underlying truth wind speeds are used in this section without regard for specific CYGNSS sampling patterns or measurement errors.

Fig. 7 plots the mean wind speed, wind speed range (max–min), and standard deviation in the "steady state" (August 6, 12 P.M.) status of the simulate cyclone, for time intervals of 30 and 60 min. The 30-min period includes seven wind speed sam-

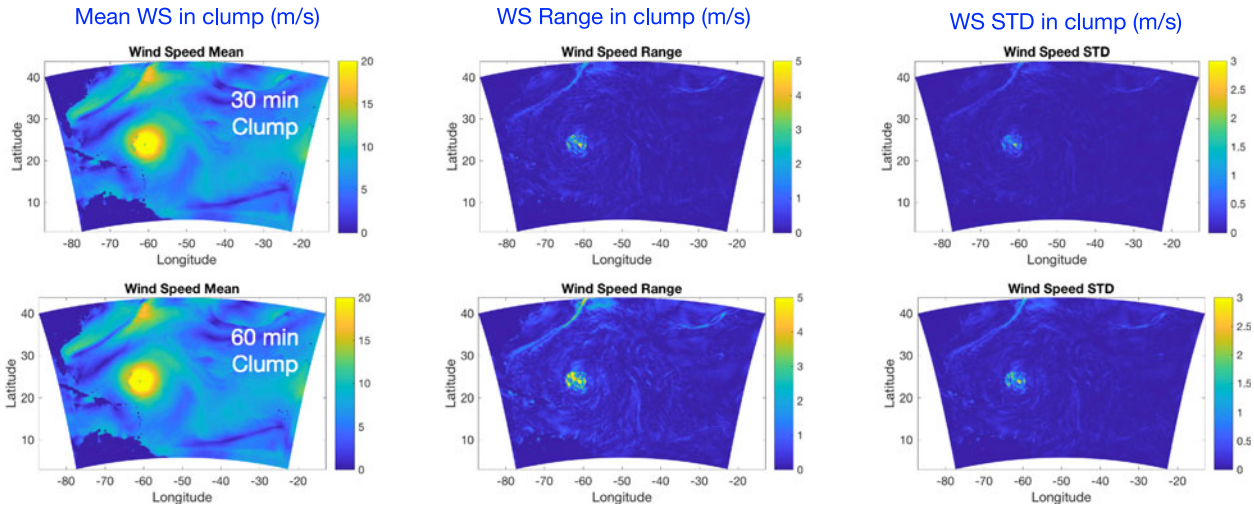

Fig. 7. Wind speed mean, wind speed range, and standard deviation over 30 and 60 min time intervals (August 6, 12 P.M., steady-state status of cyclone).

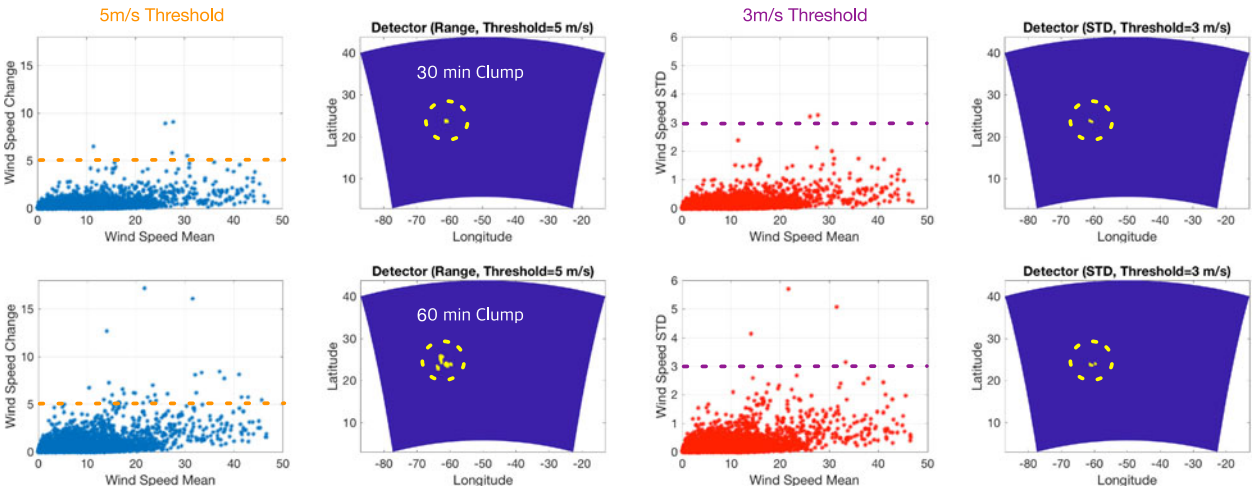

Fig. 8. Convection detector using "clump" analysis in both 30- and 60-min clumps (August 6, 12 P.M., steady-state status of cyclone, and thresholds 5 m/s for wind speed range detector and 3 m/s for standard deviation detector).

ples (12:00 P.M., 12:05 P.M., 12:10 P.M., 12:15 P.M., 12:20 P.M., 12:25 P.M., and 12:30 P.M.), with a proportionately larger number for the longer time intervals. Mean wind speeds for the two clump durations are largely similar, but the wind speed range and standard deviation increase for longer time intervals in regions near the storm.

Fig. 8 plots wind speed change and standard deviation, respectively, versus the mean wind speed for all 25-km cells in the spatial domain considered. Larger wind speed ranges again occur over the longer time interval, with only a moderate relation to the mean wind speed observed. Given the desire to "detect" particular spatial points as containing convective activity, thresholds of 5 m/s for the wind speed range and 3 m/s for the wind speed standard deviation were adopted and used to produce the detections shown in Fig. 8. For the 30-min clumps (total 240 grid cells), 12.92% (31 cells) and 1.67% (4 cells) of grid cells were detected by the wind speed range method and the wind speed standard deviation method, respectively. For the 60-min clumps, 2.08% (5 cells) and 0.83% (2 cells) of grid dells were detected. The correlation of the detected regions with the known cyclone location suggest that a simple threshold on wind speed range or standard deviation of winds in a given grid cell could be used to provide an initial detector for convective activity. Both methods are examined with on-orbit CYGNSS measurements in what follows.

IV. Analyses With CYGNSS Measurements

Attempting to detect convective activity using CYGNSS on-orbit measurements requires consideration of CYGNSS measurement errors, which will inherently contribute to both the range and the standard deviation of the wind speeds reported within a temporal clump. The wind speed retrieval algorithm of the CYGNSS mission is designed to achieve an average rms error of $\sim$1.6 m/s for wind speed $<$20 m/s [8], with higher error levels at higher wind speeds. The fact that CYGNSS

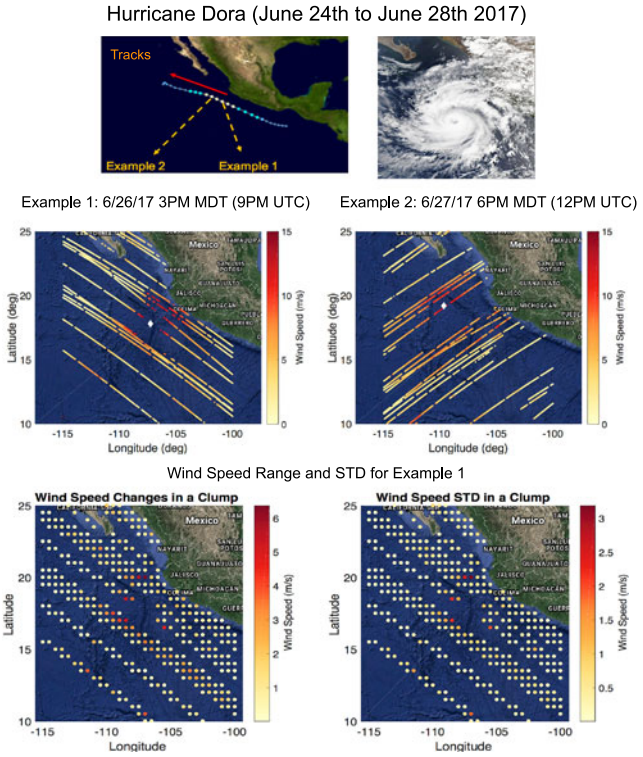

Fig. 9. Hurricane Dora (June 24–June 28, 2017) in East Pacific Ocean (track and two examples with CYGNSS L2 measurements) and wind speed range and standard deviation in 0.5° grid cells over 1 h for Example 1.

measurement errors vary with wind speed suggests that the detection threshold should be designed to increase with the mean wind speed. However for this initial examination, a fixed detection threshold independent of wind speed is applied. It is also noted that the CYGNSS wind speed retrieval algorithm continues to undergo revision at the time of writing, including efforts to address systematic errors due to GPS transmitter antenna patterns, CYGNSS receive antenna patterns, spacecraft attitude, and other factors. These errors contribute to the performance of the rapid revisit analyses reported.

The first analysis investigates detections for Hurricane Dora (June 24–June 28, 2017) in the East Pacific Ocean, a Category 1 hurricane described as having a maximum wind speed of 90 mi/h. The storm track from June 24 (Southeast) to June 28 (Northwest) and an optical image from the GOES-16 satellite are illustrated in the upper plots of Fig. 9. The directions of CYGNSS overpasses on June 26 3 P.M. MDT (9 P.M. UTC) and June 27 6 A.M. MDT (12 P.M. UTC) (called examples 1 and 2, respectively) are also indicated. The lower portions of Fig. 9 illustrate the resulting CYGNSS wind speed measurements (version 2.0), with the white diamond in each plot indicating the storm center at the time of the overpass. High wind speeds measurements near the storm center are observed in both cases. Fig. 9 further plots the wind speed range and standard deviation in the two examples. Larger wind speed changes (with a maximum of 13 m/s wind speed change) and standard deviations around the cyclone are observed, with reduced values near the storm eye. Note the standard deviation metric should be preferable as a detector due to its advantage of mitigating measurement noise as compared to the wind speed range, since all samples are used in the computation of the standard deviation as compared to the maximum and minimum values used in computing the range. Given the similarity of the results from the two detection approaches in Fig. 9, the standard deviation for clump analysis will be emphasized in later examples.

Figs. 10 and 11 provide additional examples in the West Atlantic and East Pacific Oceans, respectively. In each example, the upper left plot illustrates wind speeds obtained from NASA's Modern-Era Retrospective Analysis for Research and Applications (MERRA-2) [9] on September 30, 2017 at 5 P.M. and 8 P.M. UTC, respectively. Hurricane Maria, which ultimately evolved into an extratropical cyclone over the far northern Atlantic by September 30, is present on the upper portion of the image in the Atlantic case, but was not sampled extensively by CYGNSS. The remaining figures provide mean wind speeds from CYGNSS observations during a 1-h period (upper right) and the resulting standard deviation of winds (lower left). Standard deviations were computed using the more than ten independent wind speed measurements (with a maximum of ∼61 samples) for the points included in the figure. After applying a threshold of 3 m/s on the standard deviation of wind speed, the resulting detected point(s) are shown in the lower right plots. Section V describes attempts to associate these detections with other sources of information on convective activity.

V. Comparisons to Convective Activity Maps

In order to assess the proposed detection method, it is important to compare the results with other sources of information on convective activity. Convective activities are typically associated with cyclones or with frontal boundaries [10], and several approaches have been reported for the identification of these regions [11], [12]. Here, two methods are considered using either model winds [13] or using model temperatures [14]. For the wind-based method, the gradient of the wind direction or speed is used since significant wind speed/direction changes at frontal boundaries are usually observed. The amplitude of the spatial gradient of the wind direction ($|\nabla\phi_{\text{wind}}|$) was used for this analysis

$$|\nabla\phi_{\text{wind}}| = \left\{ \begin{array}{ll} \left|\nabla \tan^{-1}\left(V_{10}/U_{10}\right)\right| & \text{for } U_{10} > 0 \text{ m/s} \\ \left|\nabla \tan^{-1}\left(-V_{10}/U_{10}\right)\right| & \text{for } U_{10} < 0 \text{ m/s} \end{array} \right\} \tag{1}$$

where U_{10} (10-m eastward wind) and V_{10} (10-m northward wind) represent the MERRA-2 wind vector. This formula addresses the branch cut at the wind direction boundaries since changes in from wind direction 180° to −180° will appear as artificial frontal boundaries.

The temperature-based method uses the thermal frontal parameter (TFP), which expresses the gradient of the magnitude of the gradient of the temperature, resolved into the direction of the gradient [15]

$$\text{TFP} = -\nabla\left|\nabla\theta_w\right| \cdot \frac{\nabla\theta_w}{\left|\nabla\theta_w\right|} \tag{2}$$

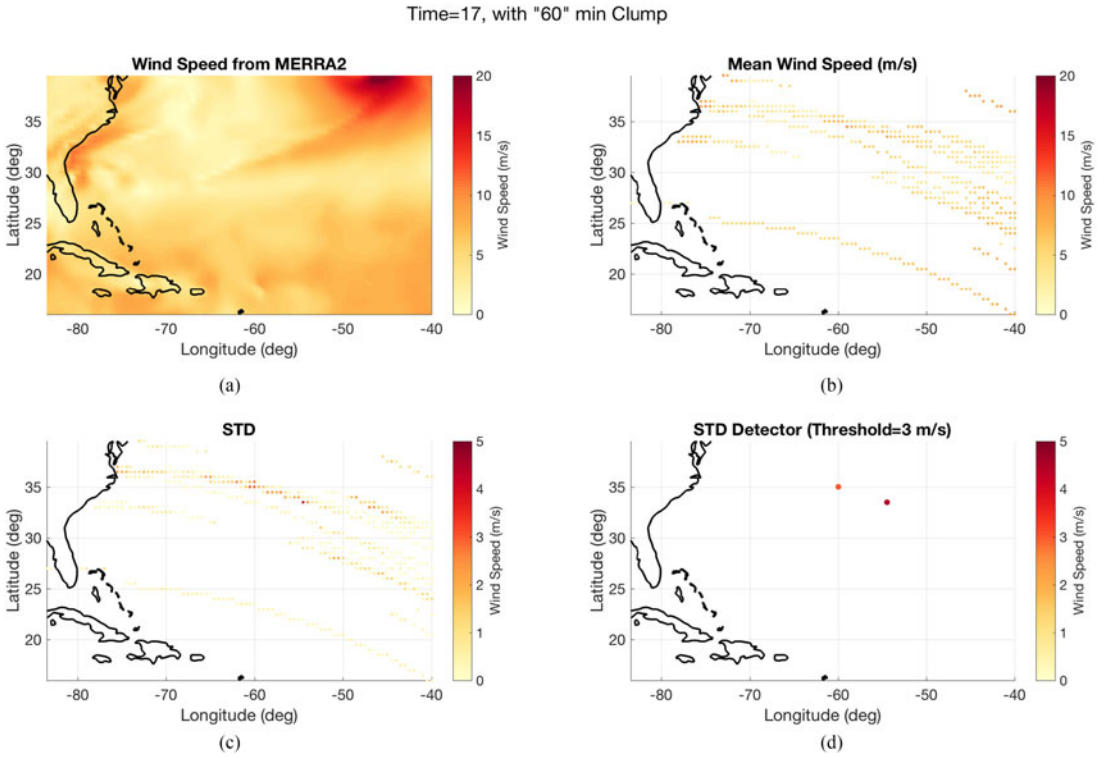

Fig. 10. First example using wind speed standard deviation method with 3 m/s threshold in 60-min clump duration. (a) Wind speeds in the West Atlantic Ocean (5 P.M. UTC) using MERRA-2 reanalysis dataset from NASA on September 30, 2017. (b) Mean wind speeds from CYGNSS observations during a 1-h period. (c) Standard deviation of CYGNSS wind speed. (d) Points having standard deviation of wind speed greater than 3 m/s.

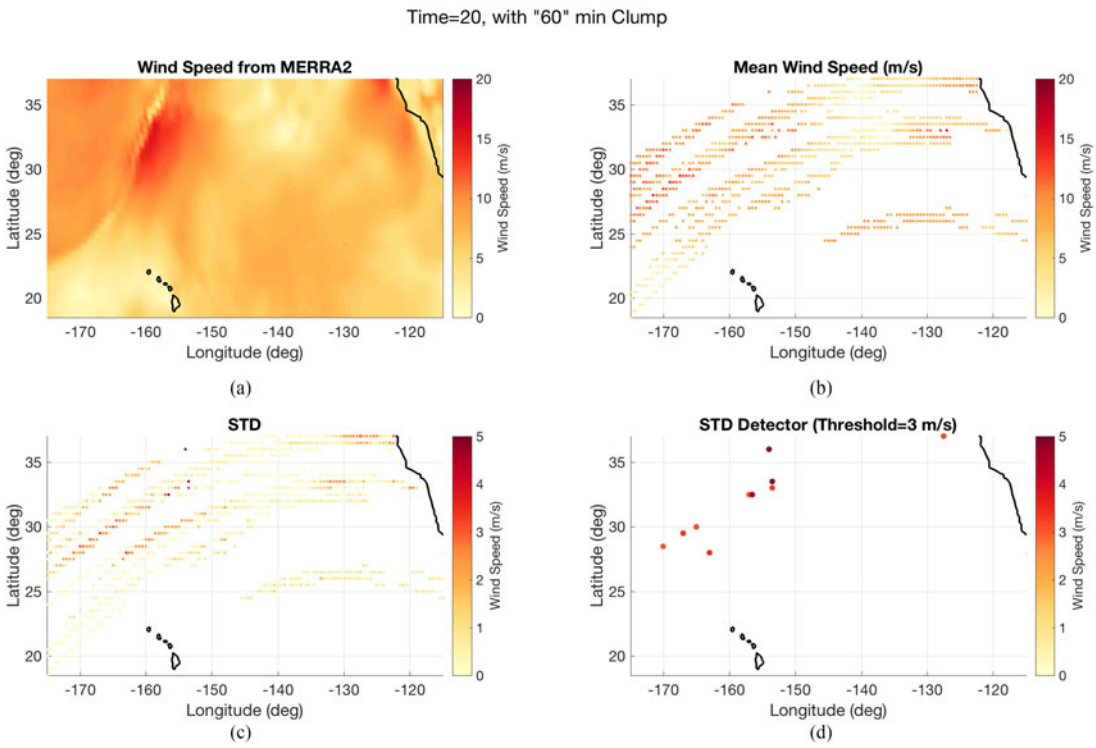

Fig. 11. Second example using wind speed standard deviation method with 3 m/s threshold in 60-min clump duration. (a) Wind speeds in the East Pacific Ocean (8 P.M. UTC) using MERRA-2 reanalysis dataset from NASA on September 30, 2017. (b) Mean wind speeds from CYGNSS observations during a 1-h period. (c) Standard deviation of CYGNSS wind speed. (d) Points having standard deviation of wind speed greater than 3 m/s.

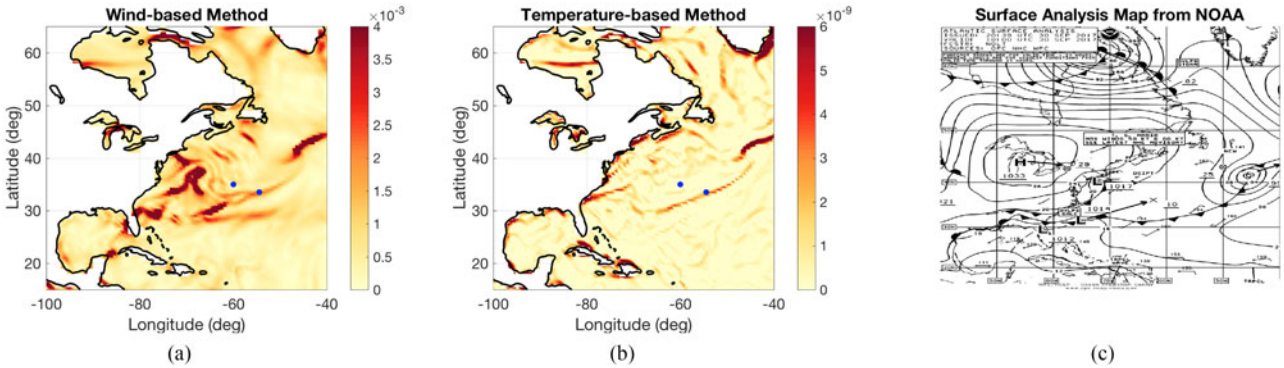

Fig. 12. CYGNSS detector results (blue dots, using wind speed standard deviation method with 3 m/s threshold in 60-min clump duration) with convection activity maps in West Atlantic Ocean. (a) Wind direction gradient amplitude (unit: degree per meter, September 30, 2017 at 5 P.M. UTC). (b) |TFP| (unit: Kelvin per square meter). (c) Surface analysis data from NOAA (September 30, 2017 at 6 P.M. UTC).

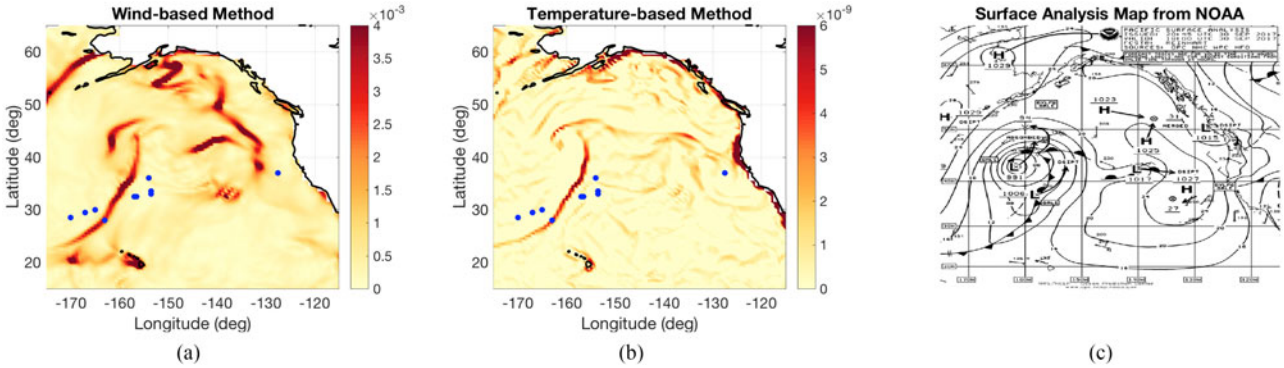

Fig. 13. CYGNSS detector results (blue dots, using wind speed standard deviation method with 3 m/s threshold in 60-min clump duration) with convection activity maps in East Pacific Ocean. (a) Wind direction gradient amplitude (unit: degree per meter, September 30, 2017 at 8 P.M. UTC). (b) |TFP| (unit: Kelvin per square meter). (c) Surface analysis data from NOAA (September 30, 2017 at 6 P.M. UTC).

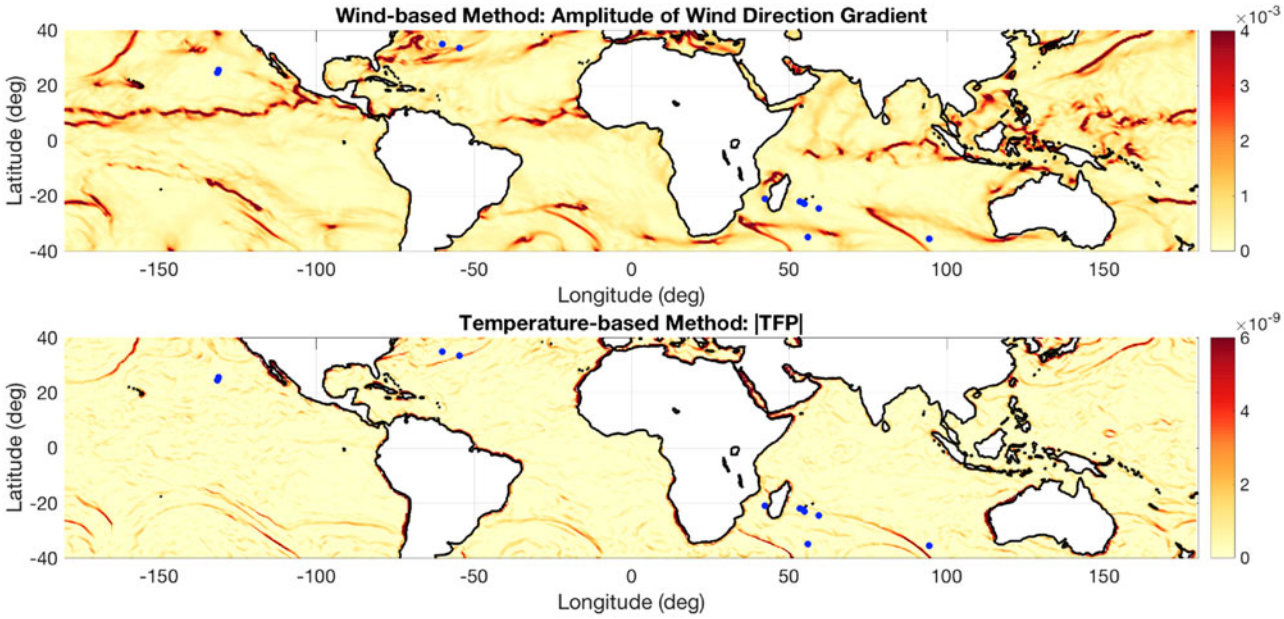

Fig. 14. CYGNSS detected points (blue dots, using wind speed standard deviation method with 3 m/s threshold in 60-min clump duration) with global convection activity map from amplitude of wind direction gradient (upper, unit: degree per meter) and |TFP| (lower, unit: Kelvin per square meter) using 1 h of CYGNSS measurements (September 30, 2017 at 5 P.M. UTC).

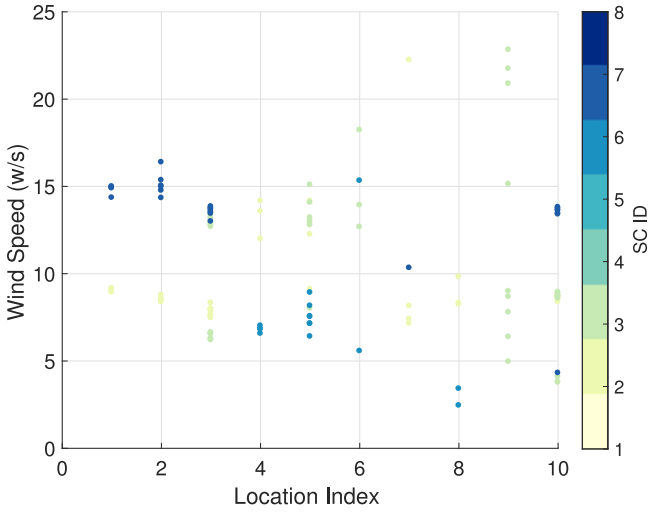

Fig. 15. Wind speed distribution of the detected ten locations in the East Pacific Ocean (see Fig. 13) color coded by spacecraft ID.

where θ_w is the wet-bulb potential temperature reported by MERRA-2.

Frontal boundaries typically appear in this quantity as deviations from zero, so the images to follow will be of the absolute value of the TFP with a colorscale from 0 to 6×10^{-9} unity. No other masking techniques or filters for the frontal information were considered in this initial work.

Figs. 12 and 13 plot the resulting wind direction gradient amplitude (left), TFP amplitude (middle), and frontal boundaries reported from a NOAA surface analysis (right) for measurements on September 30, 2017 at 5 P.M. UTC and at 8 P.M. UTC, respectively (and in distinct locations). The surface analysis data are available every 6 h from NOAA as an image product only. The results from both the wind and temperature methods correlate well with the frontal boundaries reported in the surface analysis, although the temperature-based method appears to achieve a better match. Both the wind and temperature methods were used in what follows to match up with CYGNSS rapid revisit method detections. Figs. 12 and 13 also compare both the wind- and temperature-based convection indicators with CYGNSS detector results (blue dots). CYGNSS detected locations show an encouraging correlation to apparent frontal locations obtained from the wind and temperature indicators.

Fig. 14 provides similar matchups over a larger spatial region, and again shows a reasonable match to indicated frontal boundaries. The total number of grid points examined during 60 min in this simulation was 50 623, from which only 11 samples (0.0217%) were detected. Fig. 15 provides more detailed information for each of the ten detected points in Fig. 13 by plotting all CYGNSS wind speeds reported over the examined 60-min time period. Measurements are also additionally color coded by the CYGNSS spacecraft number in order to highlight any systematic effects due to differing spacecraft. The results show wind speed ranges from 4 to 18 m/s over this period, but also show clear evidence of residual differences between spacecraft. The results in general highlight the potential of the proposed approach, but also suggest that larger scale analyses must await continued progress in the reduction of systematic errors in CYGNSS wind speed retrievals.

VI. Conclusion

The CYGNSS mission provides wind speed products that exhibit temporally clumped properties that can potentially serve as indicators of convective activity. These properties were investigated using both prelaunch simulations and on-orbit measurements to clarify properties of CYGNSS sampling and to provide initial demonstration of this concept. The results suggest that a detector can be developed using a threshold on either the range or the standard deviation of winds within a temporal clump, and that the resulting detected points should provide encouraging correlations with other sources of information on frontal boundaries. Since clump durations and spacing as well as the number of CYGNSS measurements in a clump depend significantly on location (and are more favorable at higher latitudes), the detection method and its parameters, including the threshold, clump length, and spatial resolution, should be adapted depending on the location. Also, detection performance is highly dependent on the wind speed range within a clump, which is quite sensitive to the quality of wind retrievals, the clump time period, and the detection threshold. Larger scale investigations of this method will continue as ongoing improvements in CYGNSS wind speed retrievals continue, with the goal of providing a new product for the study of wind speed variations on time scales of 1 h or less and a grid resolution of 0.25°.

References

[1] C. Ruf *et al.*, "CYGNSS: Enabling the future of hurricane prediction [remote sensing satellites]," *IEEE Geosci. Remote Sens. Mag.*, vol. 1, no. 2, pp. 52–67, Jun. 2013.

[2] S. Gleason *et al.*, "New ocean winds satellite mission to probe hurricanes and tropical convection," *Bull. Amer. Meteorol. Soc.*, vol. 97, no. 3, pp. 385–395, 2016.

[3] M. Portabella *et al.*, "Rain effects on ASCAT-retrieved winds: Toward an improved quality control," *IEEE Trans. Geosci. Remote Sens.*, vol. 50, no. 7, pp. 2495–2506, Jul. 2012.

[4] T. J. Kilpatrick and S. P. Xie, "ASCAT observations of downdrafts from mesoscale convective systems," *Geophys. Res. Lett.*, vol. 42, no. 6, pp. 1951–1958, Mar. 2015.

[5] K. E. Hoover, J. R. Mecikalski, T. J. Castillo, T. J. Lang, X. Li, and T. Chronis, "Use of an end-to-end-simulator to analyze CYGNSS," *J. Atmos. Ocean. Technol.*, vol. 35, no. 1, pp. 35–55, Jan. 2018.

[6] G. S. Elsaesser and C. D. Kummerow, "A multisensor observational depiction of the transition from light to heavy rainfall on subdaily time scales," *J. Atmos. Sci.*, vol. 70, no. 7, pp. 2309–2324, Jul. 2013.

[7] D. S. Nolan, R. Atlas, K. T. Bhatia, and L. R. Bucci, "Development and validation of a hurricane nature run using the joint OSSE nature run and the WRF model," *J. Adv. Model. Earth Syst.*, vol. 5, no. 2, pp. 382–405, Jun. 2013.

[8] M. P. Clarizia, C. S. Ruf, P. Jales, and C. Gommenginger, "Spaceborne GNSS-R minimum variance wind speed estimator," *IEEE Trans. Geosci. Remote Sens.*, vol. 52, no. 11, pp. 6829–6843, Nov. 2014.

[9] R. Gelaro *et al.*, "The modern-era retrospective analysis for research and applications, version 2 (MERRA-2)," *J. Clim.*, vol. 30, no. 14, pp. 5419–5454, Jun. 2017.

[10] D. J. Posselt, C. M. Naud, C. Bussy-Virat, and J. A. Crespo, "Assessing CYGNSS's potential to observe extratropical fronts and cyclones," *J. Appl. Meteorol. Climatol.*, vol. 56, pp. 2027–2034, 2017.

[11] S. Schemm, I. Rudeva, and I. Simmonds, "Extratropical fronts in the lower troposphere-global perspectives obtained from two automated methods," *Quart. J. Roy. Meteorol. Soc.*, vol. 141, no. 690, pp. 1686–1698, Jul. 2015.

[12] C. M. Naud, J. F. Booth, and A. D. Del Genio, "The relationship between boundary layer stability and cloud cover in the post-cold-frontal region," *J. Clim.*, vol. 29, no. 22, pp. 8129–8149, Nov. 2016.
[13] I. Simmonds, K. Keay, and J. A. T. Bye, "Identification and climatology of southern hemisphere mobile fronts in a modern reanalysis," *J. Clim.*, vol. 25, no. 6, pp. 1945–1962, Mar. 2012.
[14] T. D. Hewson, "Objective fronts," *Meteorol. Appl.*, vol. 5, no. 1, pp. 37–65, Mar. 1998.
[15] R. J. Renard and L. C. Clarke, "Experiments in numerical objective frontal analysis," *Monthly Weather Rev.*, vol. 93, no. 9, pp. 547–556, Sep. 1965.

Jeonghwan Park received the B.S. degree in electrical engineering from Yonsei University, Seoul, South Korea, in 2006, the M.S. degree in electrical engineering from the Korea Advanced Institute of Science and Technology, Daejeon, South Korea, in 2008, and the Ph.D. degree in electrical and computer Engineering from the Ohio State University, Columbus, OH, USA, in 2017.

His research interests include GNSS-R remote sensing applications and rough surface scattering.

Joel T. Johnson (S'88–M'96–SM'03–F'08) received the Bachelor of electrical engineering degree from the Georgia Institute of Technology, Atlanta, GA, USA, in 1991, and the S.M. and Ph.D. degrees in electrical engineering from Massachusetts Institute of Technology, Cambridge, MA, USA, in 1993 and 1996, respectively.

He is currently a Professor and Department Chair with the Department of Electrical and Computer Engineering and ElectroScience Laboratory, The Ohio State University, Columbus, OH, USA. His research interests include microwave remote sensing, propagation, and electromagnetic wave theory.

Dr. Johnson is a member of commissions B and F of the International Union of Radio Science (URSI), Tau Beta Pi, Eta Kappa Nu, and Phi Kappa Phi. He was the recipient of the 1993 Best Paper Award from the IEEE Geoscience and Remote Sensing Society, was named an Office of Naval Research Young Investigator, National Science Foundation Career awardee, and PECASE award recipient in 1997, and was recognized by the U.S. National Committee of URSI as a Booker Fellow in 2002.

Yuchan Yi received the Ph.D. degree in geodetic science from The Ohio State University, Columbus, OH, USA, in 1995.

He has been working in ocean applications of satellite radar altimetry including modeling of the mean sea surface, tidal analysis, and retracking of pulse-limited waveforms. His current research focuses on the GNSS reflectometry for ocean remote sensing.

Andrew J. O'Brien received the Ph.D. degree in electrical engineering from The Ohio State University, Columbus, OH, USA, in 2009.

He is currently a Research Scientist with the ElectroScience Laboratory, The Ohio State University, where from 2005 to 2009, he was a Graduate Research Associate, and worked in the area of adaptive GNSS antenna arrays and precise GNSS receivers on complex platforms. His primary research focus is currently in the area of spaceborne GNSS remote sensing using CYGNSS, TDS-1, and SMAP. His other research activities include GNSS antenna arrays, adaptive antenna electronics, airborne geolocation, and radar systems. He is a member of the CYGNSS Science Team, and has supported development of end-to-end simulations as well as engineering activities.